

## Article

# Preparation and Modification of Rape Straw Biochar and Its Adsorption Characteristics for Methylene Blue in Water

Jiao Chen <sup>1</sup>, Chenghan Tang <sup>2</sup>, Xiaoyuan Li <sup>1</sup>, Jieyu Sun <sup>1</sup>, Yujie Liu <sup>2</sup>, Wen Huang <sup>2</sup>, Aojie Wang <sup>2</sup> and Yixin Lu <sup>1,2,3,\*</sup>

<sup>1</sup> School of Materials and Environmental Engineering, Chengdu Technological University, Chengdu 611730, China

<sup>2</sup> Faculty of Geosciences and Environmental Engineering, Southwest Jiao Tong University, Chengdu 611756, China

<sup>3</sup> State Environmental Protection Key Laboratory of Synergetic Control and Joint Remediation for Soil & Water Pollution, Chengdu 610059, China

\* Correspondence: yxlu61@163.com; Tel.: +86-159-2862-8507

**Abstract:** To solve the double problems of methylene blue (MB) pollution in water and waste of straw resources, rape straw biochar (RSB<sub>600</sub>) was made by thermal decomposition of discarded rape residues at 600 °C, and modified RSB<sub>600</sub>(M-RSB<sub>600</sub>) was prepared after treatment with NaOH for MB adsorption. The physicochemical properties, MB adsorption properties and mechanism of RSB<sub>600</sub> and M-RSB<sub>600</sub> were studied. According to the experimental findings, M-RSB<sub>600</sub> has stronger aromaticity, higher hydrophilicity, and more polarity than RSB<sub>600</sub>. Under the same adsorption conditions, M-RSB<sub>600</sub> obtained better MB adsorption effect with less dosage. The MB equilibrium adsorption capacity of M-RSB<sub>600</sub> reached 268.46 mg/g, which was 65.6% higher than that of RSB<sub>600</sub>. The quasi-second-order kinetic model better described the adsorption kinetics of MB on RSB<sub>600</sub> and M-RSB<sub>600</sub> ( $R^2 > 0.98$ ), and the Freundlich and Temkin models better described the adsorption isotherms ( $R^2 > 0.95$ ). The adsorption process was spontaneous, internal heat and entropy driven multilayer adsorption, dominated by chemical adsorption, specifically involving multiple interaction mechanisms, including electrostatic adherence, hydrogen-bond,  $\pi$ - $\pi$  bond and ion-exchange. The results demonstrated that NaOH modification obviously improved the structure of RSB and make it had better adsorption and regeneration performance. M-RSB<sub>600</sub> can be utilized as the ideal substance for effectively removing MB from effluent.

**Citation:** Chen, J.; Tang, C.; Li, X.; Sun, J.; Liu, Y.; Huang, W.; Wang, A.; Lu, Y. Preparation and Modification of Rape Straw Biochar and Its Adsorption Characteristics for Methylene Blue in Water. *Water* **2022**, *14*, 3761. <https://doi.org/10.3390/w14223761>

Academic Editor: Saglara S. Mandzhieva

Received: 9 October 2022

Accepted: 15 November 2022

Published: 19 November 2022

**Publisher's Note:** MDPI stays neutral with regard to jurisdictional claims in published maps and institutional affiliations.



**Copyright:** © 2022 by the authors. Licensee MDPI, Basel, Switzerland. This article is an open access article distributed under the terms and conditions of the Creative Commons Attribution (CC BY) license (<https://creativecommons.org/licenses/by/4.0/>).

**Keywords:** biochar; rape straw; methylene blue; modification; adsorption mechanism

## 1. Introduction

Methylene blue (MB), an azo organic dye with excellent resistance to acids and bases, has a complex structure that is stable in air and not susceptible to chemical changes and is widely used in biomedical, dyeing, leather, paper and other industries [1]. The dye wastewater produced during the production and use of MB is characterized by high concentration, high chroma, high pH, difficult degradation and many changes. The water's chroma will alter, its organic pollutant content will rise, and its amount of dissolved oxygen will decrease if it is discharged directly into natural water without strict treatment [2]. When its concentration reaches a certain level, it can cause massive death of the aquatic plants and animals and damage the aquatic ecosystem. In addition, MB can cause irreparable damage to human eyes, and can also cause heart rate rise, vomiting, shock, pallor disease, jaundice, Heinz corpuscle disease, tissue necrosis and other diseases. Long-term exposure or enrichment in human body can cause cancer [3]. Finding a low-cost, effective, and ecologically friendly method to handle MB dye effluent is therefore vital.

Currently, advanced oxidation [4], photocatalysis [5], membrane technology [6,7] and adsorption [8,9] are the key techniques for eliminating organic contaminant from water. Adsorption method is one of the most popular methods, mainly because of its wide range of use, good treatment effect, easier practical operation, lower treatment cost, not easy to produce secondary pollutants, etc. The commonly used MB adsorbents mainly include activated carbon series [10], biochar series [11], hyper-crosslinked hydroxylated polystyrenes [12], leaves [13], quality [14], zeolitic imidazole framework [15], waste phosphorus [16], etc. Among them, biochar, such as charcoal, is a black solid with high carbon content produced by pyrolysis of biomass but with a difference from charcoal. This is mainly because the production process of biochar requires not only strict restriction of the oxygen content in the air but also strict control of the temperature and time of pyrolysis. It not only has low raw material price and simple preparation process but can also form a unique surface and internal structure. Therefore, the preparation of biochar from waste biomass for MB adsorption has become a research hotspot [17]. The biomass raw materials commonly used for preparing biochar mainly include plant sources, animal sources, sludge sources, etc. Plant-derived materials include rice husk [18], waste bamboo [19], eucalyptus camulensis [20], cassava peel [21], cotton residues [22], microalga residue [23], etc. Most of them contain abundant lignocellulose, so the carbon content of the prepared biochar is relatively high. The preparation of biochar from animal feces can not only reduce fecal pollution but also provide a new way for the reuse of fecal resources. Therefore, it has attracted attention in recent years [24]. As a by-product of the biological treatment method, the surplus sludge has a huge output, which is enriched with many perishable organic matter and toxic and harmful substances. Making biochar is a novel treatment method [25]. Since biochar is produced using a variety of source materials and preparation techniques, it has heterogeneous physical and chemical properties that affect how well it adsorbs contaminants from water [26]. As a result, the sector of wastewater treatment for printing and dyeing has an urgent need for the development of novel, effective, and affordable biochar materials and preparation techniques.

Rape is one of the most important oil crops in China, accounting for about one-fourth of the world's planting area, ranking first in the world. Since the 1990s, the planting area of rape has accounted for about 50% of the total planting area of various oil crops in China [27]. The amount of rape straw produced during rape planting and processing is huge every year, which can reach  $2 \times 10^7$  t/a, becoming a large agricultural by-product. With the continuous improvement of rural living facilities, coal, liquefied gas, electricity, biogas and other energy sources are gradually popularized in rural areas, and the traditional fuel value of rapeseed straw is gradually lost. In addition, due to the problems of scattered planting, large volume, high processing cost and the presence of anti-nutritional factors such as erucic acid and glucosinolate, the utilization rate of waste rape straw as fertilizer and feed is low in recent years. A large number of stalks were discarded or burned in the open air without effective utilization, resulting in serious resource waste and environmental pollution [28]. Therefore, it has become an urgent need for the sustainable development of the rape industry to explore new methods of the efficient utilization of abandoned rape straw. Rape straw can be utilized as the preferred raw material for making biochar since it is simple to obtain and abundant in organic materials. However, at present, there are few reports on the preparation of biochar from rape straw and its application to MB adsorption after modification, and its adsorption performance, adsorption influencing factors and adsorption mechanism are still not clear.

Therefore, the purposes of this study were to: (1) use waste rape straw as raw material to prepare biochar and modify it and to explore the structural characteristics of biochar before and after modification; (2) investigate the feasibility and influencing factors of removing MB from aqueous solution by rape straw biochar adsorption and (3) analyze the characteristics and mechanism of its adsorption behavior by means of kinetics, isotherm, thermodynamic model and FTIR analysis. The outcomes are anticipated to offer

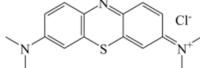
both a novel technique for the resource-efficient utilization of waste rape straw and a fresh approach for the elimination of MB from aqueous systems.

## 2. Materials and Methods

### 2.1. Main Reagents and Solutions

The MB ( $C_{16}H_{18}ClN_3S$ ), HCl (hydrochloric acid), NaOH (sodium hydroxide) and  $C_2H_5OH$  used in the experiment were all acquired from Chengdu, China's Kelong Chemical Co., Ltd., and were all analytical pure. Table 1 displays the primary physical and chemical characteristics of MB. Prepare 1000 mg/L MB mother liquor and dilute it according to the actual needs before use. Prepare 1.5 mol/L NaOH solution for the modification of biochar. To change the solution's original pH, prepare a 1.0 mol/L HCl and NaOH solution. The water used in experiment was deionized water.

**Table 1.** Principal MB chemical and physical characteristics.

Chemical Formula	Molecular Weight (g/mol)	Molecular Structure	Solubility in Water (25 °C)	CAS Number
$C_{16}H_{18}ClN_3S$	319.85		10%	61-73-4

### 2.2. Preparation and Modification of Biochar

By using oxygen-limited pyrolysis, the waste rape straw that was gathered from a rape planting base in Pidou District, Chengdu City, China, was converted into biochar. After the impurities were removed, the rape straw was cleaned and dried. After being crushed, it was filtered with an 80-mesh screen to result in a product with particles smaller than 0.18 mm. Take an appropriate amount into a quartz boat to compact it and put it into a tube furnace. According to the results of preliminary experiments, the temperature was kept constant for 2 h after being heated to 600 °C at a heating rate of 20 °C/min under the protection of the nitrogen flow. The tube furnace was equipped with a tail gas collection port, and the tail gas generated in the pyrolysis process was discharged after being absorbed by alkali liquor and ethanol solution.

After heating, the tube furnace was closed, and after natural cooling, the pyrolysis solid product was taken out, ground and divided into two parts. One part of the pyrolysis product was washed with deionized water until the pH value of the supernatant was stabilized, then the supernatant was filtered out and the solid was dried in a drying oven, the dried solid was sieved through 100 mesh sieve and the sieved product was rape straw biochar (RSB) with a particle size lower than 0.15 mm, marked as RSB<sub>600</sub> and stored in a sealed and dry place; the other part of the pyrolysis product was modified with 1.5 mol/L NaOH. The other part of the pyrolysis product was modified with 1.5 mol/L NaOH solution, and 100 mL of the above concentration of NaOH solution was added to each 1 g of the pyrolysis solid product, placed in a constant temperature shaker, and shaken at 25 °C and 150 r/min for 12 h. After that, the residue was filtered out, and the residue was washed with deionized water until the pH value of the supernatant was stabilized, then the supernatant was filtered out and the solid was dried and the dried solid was passed through a 100-mesh sieve. The dried solid was passed through a 100-mesh sieve, and the sieved product was the modified rape straw biochar with a particle size lower than 0.15 mm, labeled as M-RSB<sub>600</sub>. The prepared biochar was sealed and stored in a dryer for standby. The specific preparation process was shown in Figure 1.

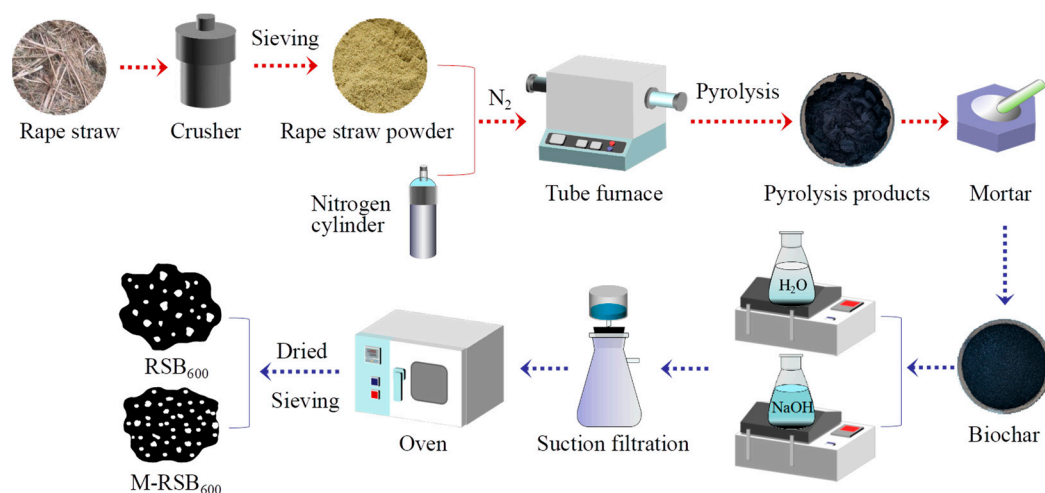


**Figure 1.** Preparation and modification process of RSB.

### 2.3. Experimental Scheme

Take several 250 mL conical flasks and measure 100 mL of MB solution of certain concentration and pH using a measuring cylinder, then add a certain amount of RSB and shake it at a certain temperature with a constant temperature of 150 r/min for a certain time. In the study of the relationship between the MB adsorption effect and solution pH, 80 mg/L of MB solution was added to the conical flask and the initial pH of the solution was adjusted using NaOH and HCl with a gradient set in the range of  $-11$ . The amount of RSB<sub>600</sub> and M-RSB<sub>600</sub> was 0.3 g/L, and the reaction was ensured at a constant temperature of 25 °C with an oscillation time of 180 min. In addition, the concentration of MB solution involved in the reaction was adjusted to 80 mg/L, the initial pH of the solution was 10, the dosage of RSB<sub>600</sub> and M-RSB<sub>600</sub> was 0.1–1.0 g/L, the reaction temperature was 25 °C and the oscillation time was 180 min, so as to investigate the relationship between the MB removal rate in the RSB/MB system and the dosage of the RSB relationship. The reaction time also has kind of important effect on the adsorption rate of MB. In examining the relationship between the MB adsorption effect and reaction time, MB at a concentration of 80 mg/L was added to a conical flask, and the pH of the solution was mediated using HCl and NaOH to make pH = 10. Immediately afterwards, 0.5 g/L of RSB<sub>600</sub> and 0.3 g/L of M-RSB<sub>600</sub> were put into the conical flasks, and the reaction temperature was kept constant at 25 °C and shaken continuously for 5–180 min. The initial concentration of the pollutant and the temperature of the reaction affect the adsorption process of MB and therefore have an important influence on the adsorption effect. Therefore, in studying the relationship between them, a series of MB concentrations put into the conical flask reaction were set in the range of 70–150 mg/L, the pH of the solution was adjusted to 10 using HCl and NaOH, 0.5 g/L of RSB<sub>600</sub> and 0.3 g/L of M-RSB<sub>600</sub> were added, respectively, and the reaction temperature was maintained at 25–45 °C with an oscillation time of 180 min.

After the oscillation, the supernatant was centrifuged to detect the mass concentration of the remaining MB. According to the adsorption amount data under different adsorption times, the kinetic analysis was carried out. Thermodynamic and isothermal analyses were performed in accordance with the data on the quantity of adsorption at various beginning concentrations, reaction temperatures and times.

In the regeneration experiment, RSB<sub>600</sub> and M-RSB<sub>600</sub> saturated with adsorbed MB were added to 100 mL ethanol solution and oscillated at a constant temperature of 25 °C and 150 r/min for 60 min. After that, they were rinsed with deionized water. Repeat the operation 3 times. After the filtered filter residue was dried, the removal rate of MB by RSB<sub>600</sub> and M-RSB<sub>600</sub> after desorption was determined. Repeat the above operation 6 times to evaluate the regeneration performance of RSB<sub>600</sub> and M-RSB<sub>600</sub>.

## 2.4. Analysis Method

RSB's ash content was measured using a muffle furnace (SG-XL1200, Institute of Optics and Fine Mechanics, Shanghai, China). The contents of C, H, N and O in RSB were analyzed by an element analyzer (VARIO EL cube, Elementar, Hunau, Germany). Determine the specific surface area, total pore volume and mean pore diameter of RSB using a specific surface area analyzer (NOVA 4000e, Quantachrome, Florida, USA). Meanwhile, the surface morphology of RSBs (SEM analysis) was observed using a field emission scanning electron microscope (Gemini 300, ZEISS, Germany). The point of zero charge ( $\text{pH}_{\text{pzc}}$ ) was measured by a potentiometer (Zetasizer ZEN3600, Malvern Instruments, UK). FTIR can play an important role in detecting the changes of functional groups on the RSB surface before and after adsorption, mainly using a Fourier-infrared spectrometer (Nicolet 670, Thermo Fisher, USA). The mass concentration of MB in the inlet and outlet water was detected by a visible light spectrophotometer (722S, Jingke Industrial Co., Ltd., Shanghai), and the maximum absorption wavelength was 665 nm. All experiments were performed three times in parallel in this study, and the average values were taken to calculate the removal rate  $\eta$  (%) and the adsorption amount  $q_t$  (mg/g) of MB by RSB. The calculation formulas of  $\eta$  and  $q_t$  were shown in Equations (1) and (2), respectively.

$$\eta = \frac{C_0 - C_t}{C_0} \times 100\% \quad (1)$$

$$q_t = \frac{(C_0 - C_t)V}{m} \quad (2)$$

where  $C_0$  and  $C_t$  represent the mass concentration of MB in solution (mg/L), respectively, with 0 denoting the initial concentration and  $t$  denoting the concentration of MB at time  $t$ ;  $V$  represents the volume of MB solution (mL), and  $m$  represents the amount of RSB<sub>600</sub> and M-RSB<sub>600</sub> (g).

## 3. Results and Discussion

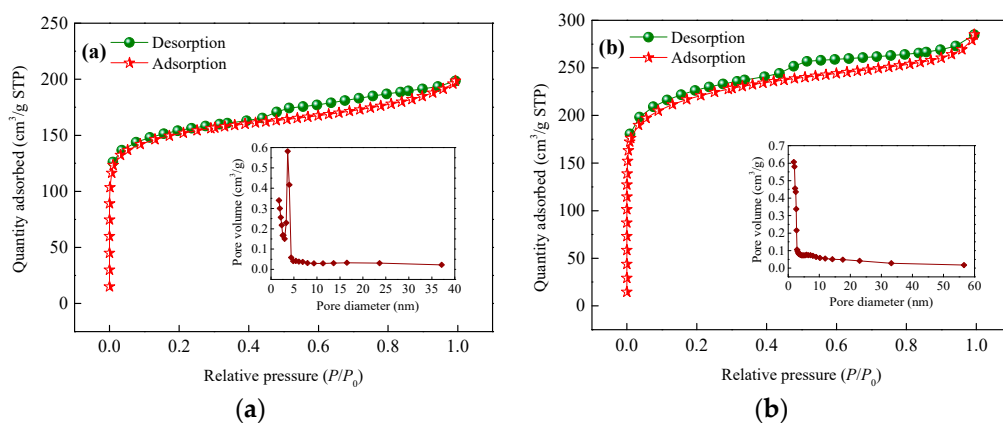
### 3.1. Structural Characteristics of RSB

Table 2 displays the primary physical and chemical characteristics of RSB<sub>600</sub> and M-RSB<sub>600</sub>. In terms of the ash content, the ash content of M-RSB<sub>600</sub> was 16.67% lower than that of RSB<sub>600</sub>. In terms of elemental composition, both kinds of biochar contained C, H, O and N, of which C was the most abundant. M-RSB<sub>600</sub> had a lower concentration of C and H than RSB<sub>600</sub> but a higher proportion of O and N. Biochar can be evaluated for its aromaticity, hydrophilicity and polarity using the H/C, O/C and (O+N)/C atomic ratios, respectively. The aromaticity of biochar decreases as the H/C atomic ratio increases. As the O/C and (O+N)/C atomic ratios increased, so did the hydrophilicity and polarity, respectively [29]. Table 2 shows that M-RSB<sub>600</sub> had lower H/C and greater O/C and (O+N)/C atomic ratios compared to RSB<sub>600</sub>, indicating that the RSB that had been modified by NaOH had stronger aromaticity and increased hydrophilicity and polarity. The oxidation of some functional groups on the surface of biochar and the rise in the proportion of oxygen-containing functional groups were both factors in the high O/C (O+N)/C atomic ratio [30]. Additionally, RSB<sub>600</sub> and M-RSB<sub>600</sub> had H/C and O/C atomic ratios that were lower than 0.1 and 0.3, respectively, demonstrating that both types of biochar have great biological stability [31]. The findings of the BET study showed that, in comparison to RSB<sub>600</sub>, M-RSB<sub>600</sub>'s surface area and total pore volume rose by 93.94% and 81.55%, respectively, whereas its average pore diameter dropped by 73.04%. According to the N<sub>2</sub> adsorption-desorption isotherm and pore size distribution curve shown in Figure 2, when  $P/P_0$  was less than 0.1, the N<sub>2</sub> adsorption capacity of RSB<sub>600</sub> and M-RSB<sub>600</sub> increased rapidly, indicating that there were abundant micropores. When  $P/P_0$  was less than 0.9, the N<sub>2</sub> adsorption curve showed a slow upward trend. When  $P/P_0$  was greater than 0.4, there was an obvious hysteresis loop, which indicated that there was a certain amount of mesoporous structure in the biochar. When  $P/P_0$  was greater than 0.9, the adsorption curve still had a certain

growth trend, indicating that there were also some macropores in RSB<sub>600</sub> and M-RSB<sub>600</sub>. RSB<sub>600</sub> had a large number of mesopores, mostly concentrated in the range of 2–5 nm. Compared with RSB<sub>600</sub>, M-RSB<sub>600</sub> had more micropores, which were mostly concentrated in the range of 1–2 nm. A similar phenomenon also appeared in the study of Shin et al. [32]. Alkali modification of biochar made from used coffee grounds with NaOH led to an increase in surface area and total pore volume, while the average pore width decreased from 5.818 nm to 3.113 nm. Novera et al. [33] modified the betel nut shells with NaOH, and found that its specific surface area and total pore volume increased compared with those before modification, but different from this study, its average pore diameter increased from 4.97 nm to 6.92 nm. Different pore development results after modification may be related to different adsorbent raw materials and modification conditions, but it can be seen that NaOH modification can obviously improve the surface structure of adsorbents.

**Table 2.** The physicochemical properties of RSB<sub>600</sub> and M-RSB<sub>600</sub>.

Analysis item	Index	RSB <sub>600</sub>	M-RSB <sub>600</sub>
Quality composition	Ash (%)	14.239	11.865
	C (%)	66.417	63.674
	H (%)	2.554	1.821
	O (%)	9.731	12.823
	N (%)	1.428	2.956
Atomic ratio	H/C	0.038	0.029
	O/C	0.147	0.201
	(O+N)/C	0.168	0.248
BET	Specific surface area (m <sup>2</sup> /g)	61.597	119.462
	Total pore volume (cm <sup>3</sup> /g)	0.168	0.305
	Average pore diameter (nm)	7.162	4.139



**Figure 2.** N<sub>2</sub> adsorption–desorption isotherm and pore size distribution curve of RSB<sub>600</sub> (a) and M-RSB<sub>600</sub> (b).

According to the SEM analysis results of RSB<sub>600</sub> and M-RSB<sub>600</sub> shown in Figure 3, both two kinds of biochar had rich pore structures, which was caused by the decomposition or precipitation of water, organic matter and other volatile components in the straw biomass during the pyrolysis process [34]. The difference was that the surface of M-RSB<sub>600</sub> showed a more lamellar structure, rougher compared to RSB<sub>600</sub>, some areas collapsed and the pores were more abundant and compact. Before the RSB was modified, some micropores were blocked by impurities that were difficult to clean with water. As a result of the insoluble materials being dissolved by NaOH during the modification process, the blocked pores were unblocked, and the oxygenic groups were revealed. The increase of oxygenic

groups in the structure of biochar increased the hydrophilicity on the one hand and improved the ion exchange capacity on the other [35]. The modification process also allowed for the removal of some ash. By NaOH etching, the pores on the surface of RSB were also made more open and numerous. Due to this, M-RSB<sub>600</sub> had better adsorption potential than RSB<sub>600</sub> due to its greater specific surface area, total pore volume and lower average pore width.

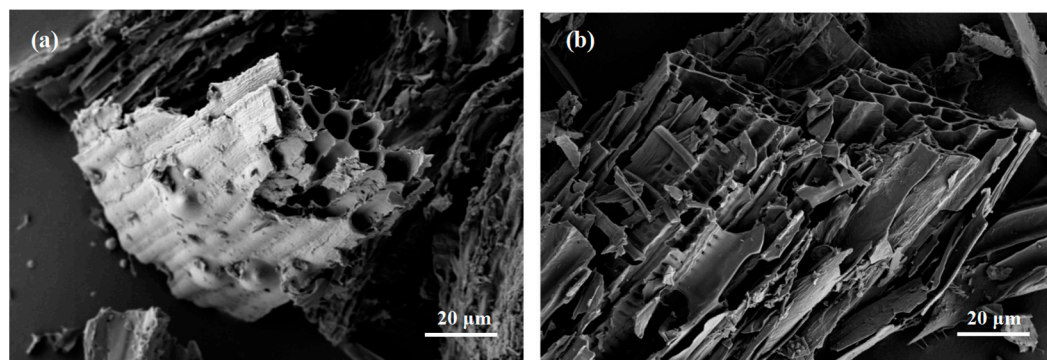


**Figure 3.** Scanning electron microscope of RSB<sub>600</sub> (a) and M-RSB<sub>600</sub> (b).

### 3.2. Analysis of Adsorption Influencing Factors

#### 3.2.1. Effect of initial pH Value of Solution

Figure 4 shows the variation of the adsorption effect of RSB on MB in the reaction system with different pH values. From the data in Figure 4, it can be judged that the removal rate and adsorption amount of MB by two types of biochar (RSB<sub>600</sub> and M-RSB<sub>600</sub>) varied with pH—specifically, the removal effect of MB by RSB<sub>600</sub> and M-RSB<sub>600</sub> increased with the increase of pH. M-RSB<sub>600</sub> demonstrated a better adsorption effect under the same pH conditions. When the pH was set to 10, the adsorption capacity and removal rate of MB by M-RSB<sub>600</sub> were 182.53 mg/g and 95.80%, respectively, which was 39.96% and 27.35% greater than RSB<sub>600</sub>. The removal impact of RSB<sub>600</sub> and M-RSB<sub>600</sub> for MB was not significantly increased when the pH was continuously raised to 11; hence, the ideal starting pH value of the solution was decided to be 10 in the subsequent studies.

This can be accounted for by the impact that the initially pH of the liquid has on the charged state of the biochar surface and the morphology of the adsorbate present. In the acidic solution, the highly protonated functional groups of RSB reduced the negatively charged active sites of RSB, which led to the weakened electrostatic attraction between RSB and the cationic form of MB in solution and inhibited the adsorption of MB. At the same time, the more H<sup>+</sup> in the solution with low pH value, the stronger the ability to compete with MB for the effective active sites involved in adsorption on RSB, which further caused a decline in the adsorption capacity of MB. The adsorption capacities of RSB<sub>600</sub> and M-RSB<sub>600</sub> for MB were, respectively, 123.66 mg/g and 74.20 mg/g lower at pH value 2 than at pH value 10. On the contrary, the positive charge density on the RSB surface decreased due to deprotonation at larger pH values, thus enhancing the electrostatic attraction to MB and promoting MB to be removed by approaching the surface of RSB. Therefore, the adsorption of MB by RSB can be maximized under alkaline conditions [36]. Novera et al. [33] used sodium hydroxide modified betel nut shells to adsorb MB from water at pH 2 to 12, the amount of MB adsorbed was lowest at pH 2 and the amount of adsorbed significantly improved with the rising of pH. However, with the gradual increase of the initial pH of the reaction solution, the adsorption effect was significantly improved. Huang et al. [37] also found that an alkaline environment was more favorable to boost the adsorption capacity of biochar when using biochar from sheep, rabbit and pig manure to remove MB from water. In addition, M-RSB<sub>600</sub> had stronger adaptability to pH changes and can still maintain a high MB adsorption effect under acidic conditions. Salah et al. [38] prepared biochar using industrial sludge as a carbon source under pyrolysis conditions at 750 °C

and then applied it for adsorption of dye cations from aqueous solutions. Their experimental viewpoint concurred that the alkaline modified biochar had a more suitable zero point charge and also concluded that the sludge-based biochar activated by KOH had a superior ability to adapt to the initial pH of the solution during the reaction.

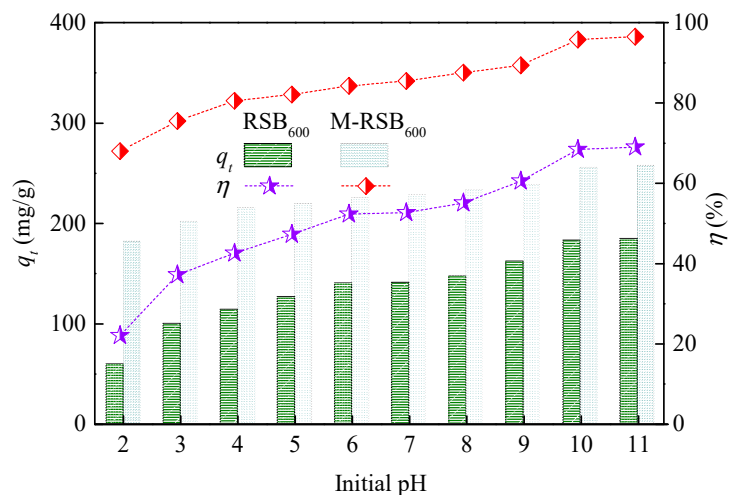


**Figure 4.** The adsorption performances under different initial pH.

Zeta potential analysis results of RSB<sub>600</sub> and M-RSB<sub>600</sub> are shown in Figure 5. It can be seen that the  $\text{pH}_{\text{pzc}}$  of RSB<sub>600</sub> and M-RSB<sub>600</sub> were 2.78 and 2.17, respectively. When the pH value of the solution was higher than the respective  $\text{pH}_{\text{pzc}}$ , the surface of the biochar was negatively charged, and the number of negative charges increased with the increase of pH, which was conducive to the adsorption of cationic MB with opposite charges in the solution. Therefore, electrostatic attraction had a great contribution to the adsorption of MB by RSB<sub>600</sub> and M-RSB<sub>600</sub>. The  $\text{pH}_{\text{pzc}}$  value of RSB<sub>600</sub> was higher than that of M-RSB<sub>600</sub>, which indicated that the amount of negative charge on the surface of RSB can be increased by NaOH modification at a lower pH, and the adsorption capacity of MB in solution was also stronger.

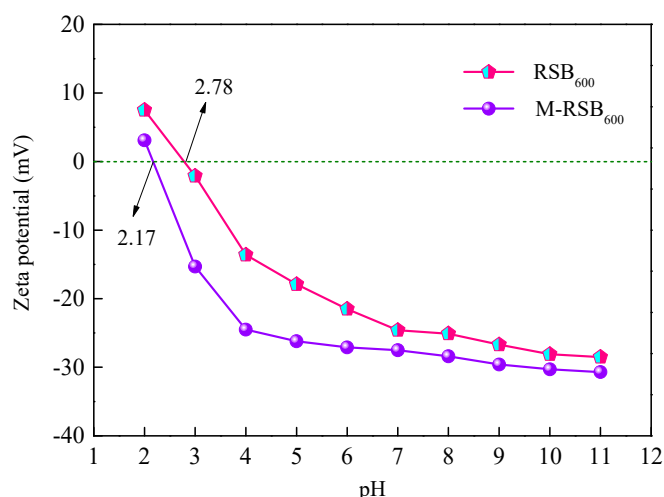


**Figure 5.** Zeta potential at different pH values.

### 3.2.2. Effect of RSB Dosage

Figure 6 depicts the MB adsorption effect at various RSB dosages. It is evident that as RSB dosage was increased, MB elimination first increased and then tended to be gentle. This is because the higher the dosage of RSB, the more active adsorption sites available

for MB were provided, so the removal rate also increased, and it did not increase significantly until the content of MB that can be adsorbed in water dropped to a lower level [39]. However, the amount of MB adsorbed by RSB, and the removal rate of MB showed the opposite change law. When the dosage of RSB<sub>600</sub> and M-RSB<sub>600</sub> reached 1.0 g/L, although the MB removal rate was 100%, the quantity of MB adsorbed was only 80 mg/g, which indicated that the high dose of RSB would result in too many adsorption sites on the biochar, which would drastically impair the adsorption capacity of the unit mass of RSB to MB when the MB content in the water was limited [40].

Therefore, the optimum dosage levels of RSB<sub>600</sub> and M-RSB<sub>600</sub> were determined to be 0.5 and 0.3 g/L. Under the optimum dosage level, the MB removal rate increased by 70.11% and 48.54% compared to that of RSB<sub>600</sub> and M-RSB<sub>600</sub> at 0.1 g/L, and the adsorption capacity increased by 0.9 and 2 times compared to that of RSB<sub>600</sub> and M-RSB<sub>600</sub> at 1.0 g/L, respectively. The adsorption capacity increased by 0.9 times and 2.2 times compared with RSB<sub>600</sub> and M-RSB<sub>600</sub> at 1.0 g/L, respectively. These RSB dosages can not only achieve good MB removal effect but also will not cause waste of biochar resources. It is worth noting that, under the same biochar dosage, the adsorption effect of M-RSB<sub>600</sub> on MB was better than that of RSB<sub>600</sub>. The study found that the M-RSB<sub>600</sub> dose with 100% MB clearance was 0.8 g/L. It can be seen that the alkali modification made RSB have a better surface structure, which can provide more active adsorption sites for MB and realize the more efficient removal of MB with less biochar dosage.

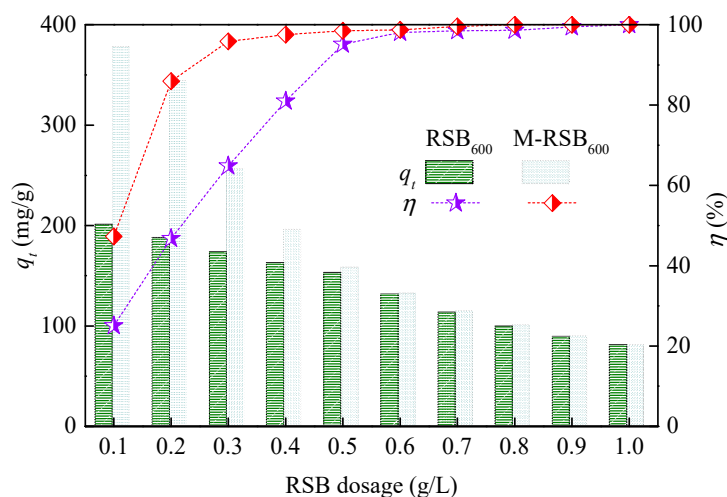


**Figure 6.** The adsorption performance under different RSB dosages.

### 3.2.3. Effect of Contact Time

Figure 7 depicts the relationship between different reaction times on the adsorption effect in the RSB/MB reaction system. In the RSB<sub>600</sub>/MB and M-RSB<sub>600</sub>/MB reaction systems, the adsorption and removal rates of MB by both biochar were proportional to the duration of the reaction within 60 min after the onset of the reaction. During the initial period of adsorption time, the RSB was able to adsorb a high amount of MB quickly; this is mainly due to the presence of a significant amounts of reactive spots helping to adsorb pollutants on the RSB surface [41]. When the reaction time between RSB and MB reached 60 min, the removal rates of MB by RSB<sub>600</sub> and M-RSB<sub>600</sub> were 93.09% and 93.86%, respectively, and the adsorption amounts were 148.94 mg/g and 250.30 mg/g. After the reaction time between RSB and MB reached a certain time, the concentration of remaining MB in water decreased, and most of the adsorption sites of RSB were occupied, resulting in no significant improvement in the removal of MB by RSB [42]. Therefore, the adsorption equilibrium time of RSB<sub>600</sub> and M-RSB<sub>600</sub> for MB was about 60 min.

Although the removal rates of MB by the two RSBs were very close, the adsorption rates were significantly different. Within 60 min after the start of the adsorption reaction,

it was observed that the adsorption rate of 7.54 mg/(g·min) for MB was significantly higher for M-RSB<sub>600</sub> than RSB<sub>600</sub> during the first 30 min, which was about 1.7 times higher than that of RSB. The adsorption rate of M-RSB<sub>600</sub> for MB was 4.17 mg/(g·min) in the last 30 min, which was still 68.05% higher than that of RSB<sub>600</sub>, although it decreased. It can be seen that when alkali-modified RSB was used to treat MB, it can not only save the material cost by reducing the dosage but also save the time cost by increasing the adsorption rate, so that the adsorption performance of RSB can be brought into full play and has good application value and potential in practice.

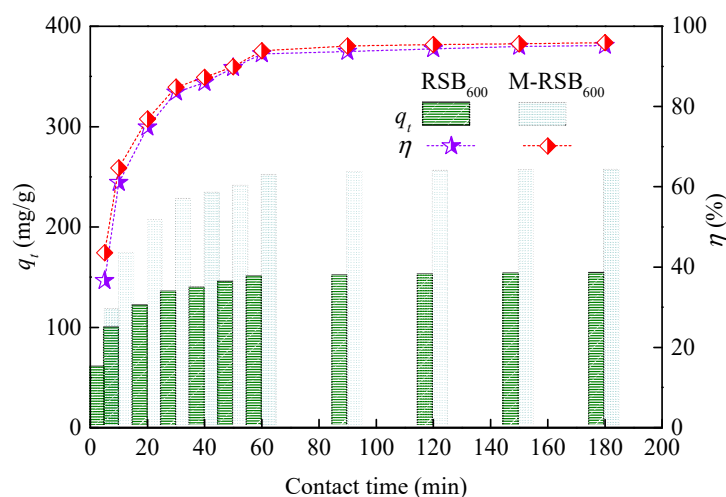


**Figure 7.** The adsorption performance under different contact times.

#### 3.2.4. Effect of Initial Concentration of MB

The correlation between the initial concentration of MB and the adsorption efficiency of RSB is illustrated in Figure 8. In this experiment, 70, 80, 90, 100, 120 and 150 mg/L were taken as the starting mass concentration of MB solution to test the adsorption ability and removal rate of MB by RSB<sub>600</sub> and M-RSB<sub>600</sub>. As shown in Figure 6, the initial concentration of MB had a very obvious effect on RSB adsorption. The clearance rate of MB in water exceeded 95% when the starting concentration of MB was lower than 80 mg/L. The clearance rate of MB rapidly reduced with the rise of the initial concentration of MB when it was above 80 mg/L. The removal rates of MB by RSB<sub>600</sub> and M-RSB<sub>600</sub> were only 59.97% and 60.37% when the starting concentration of MB reached 150 mg/L, respectively. The effluent contained high concentration of residual MB, which could not meet the discharge requirements.

In the comparative of the capacity of MB adsorption, M-RSB<sub>600</sub> presented a more outstanding result. When the starting density of MB involved in the reaction was changed from 70 mg/L to 150 mg/L, the adsorption ability of RSB<sub>600</sub> improved by 41.92 mg/g, while that of M-RSB<sub>600</sub> improved by 70.47 mg/g. Since biochar had a comparatively significant adsorption capacity and can more fully adsorb MB when the initial concentration of MB was low, the removal rate was high. When the initial concentration of MB increased, the biochar was getting close to reaching adsorption saturation. This increased the difference in MB concentration between the liquid and the solid, which increased the driving force for MB migration to the RSB, and the adsorption reaction was more complete. Consequently, MB adsorbed by RSB increased per unit mass [43]. Since the adsorption point of RSB was limited under the fixed dosage, the rate of increase in adsorption capacity would gradually slow down after reaching adsorption equilibrium. Due to this, the best adsorption effect was achieved when the starting concentration of MB was 80 mg/L without determining the optimal RSB dosage, which considered both the removal rate and the adsorption amount.

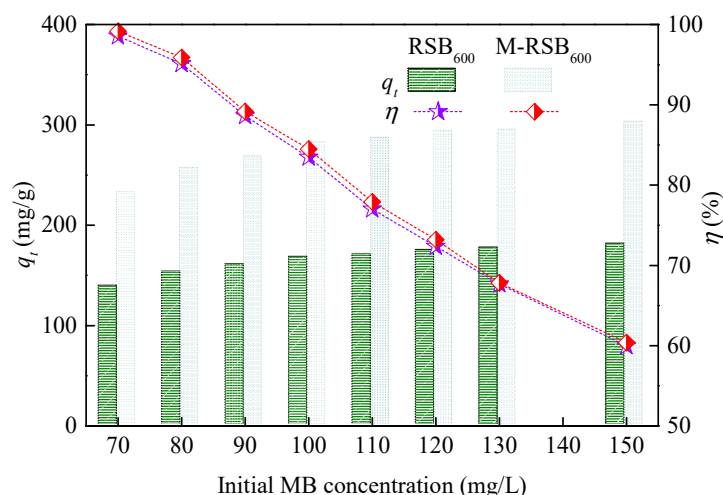


**Figure 8.** The adsorption performance under different initial MB concentrations.

### 3.3. Adsorption Kinetics

The quasi-first-order kinetic model, quasi-second-order kinetic model, intraparticle diffusion model and Elovich model [44] are used to fit the adsorption capacity data of RSB<sub>600</sub> and M-RSB<sub>600</sub> on MB under different contact times in order to analyze the adsorption kinetic characteristics of MB onto RSB in water. The fitting results are shown in Figure 9.

$$\ln(q_e - q_t) = \ln q_e - k_1 t \tag{3}$$

$$\frac{t}{q_t} = \frac{t}{q_e} + \frac{1}{k_2 q_e^2} \tag{4}$$

$$q_t = k_3 t^{0.5} + A \tag{5}$$

$$q_t = k_4 \ln t + B \tag{6}$$

where  $q_t$  and  $q_e$ , respectively, represents MB adsorption amount at time  $t$  (min) and adsorption equilibrium time (mg/g);  $k_1$ ,  $k_2$ ,  $k_3$  and  $k_4$  are the rate constants corresponding to the above kinetic models, and the units are  $\text{min}^{-1}$ ,  $\text{g}/(\text{mg}\cdot\text{min})$ ,  $\text{mg}/(\text{g}\cdot\text{min}^{0.5})$  and  $\text{mg}/(\text{g}\cdot\text{min})$ , respectively;  $A$  and  $B$  are the correlation constants.

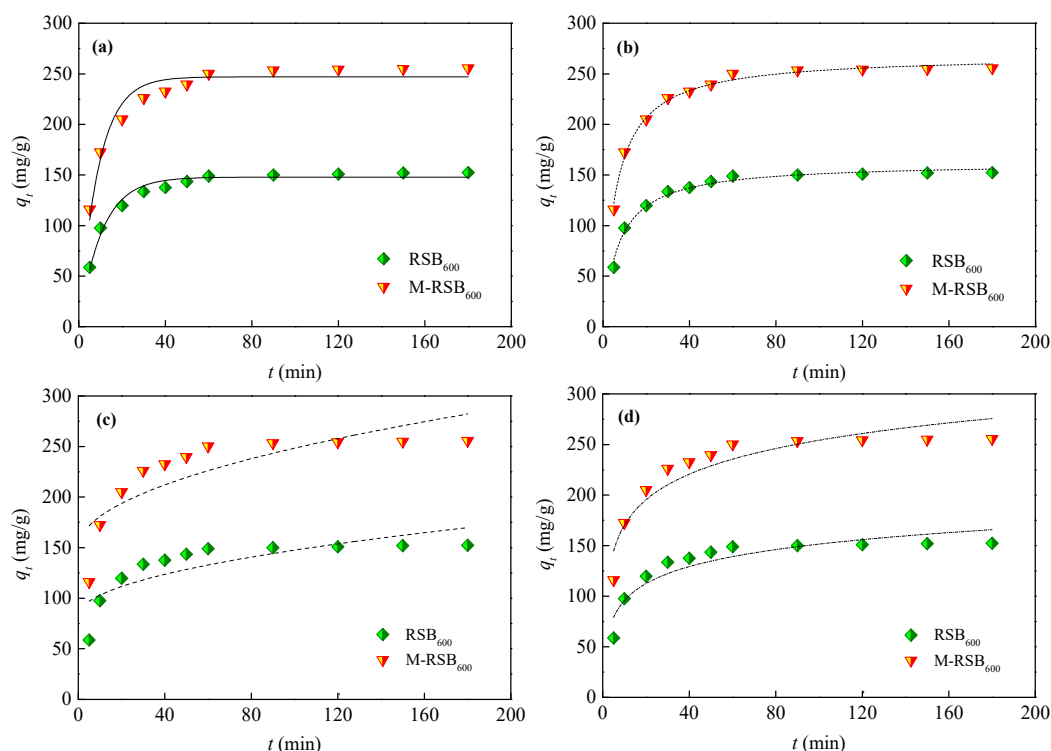


**Figure 9.** Adsorption kinetics fitting of RSB<sub>600</sub> and M-RSB<sub>600</sub> for MB: (a) quasi-first-order kinetic model, (b) quasi-second-order kinetic model, (c) intraparticle diffusion model and (d) Elovich model.

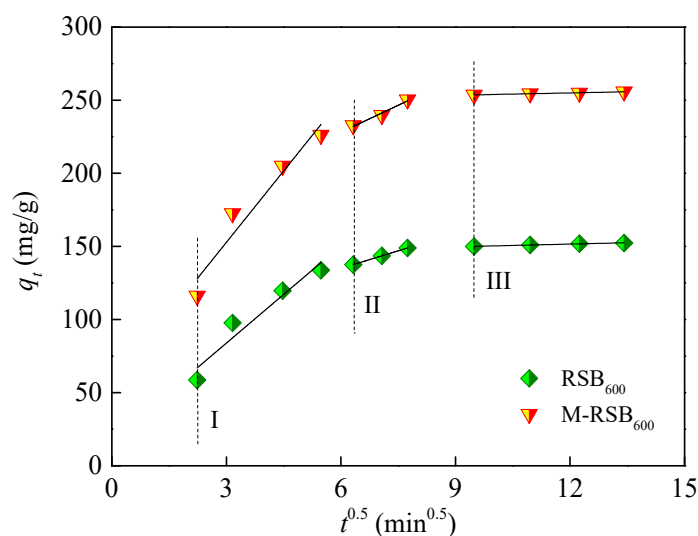
The fitting parameters for the four adsorption kinetic models discussed previously are shown in Table 3. When the quasi-second-order kinetic model was used to fit the adsorption experimental data, the determination coefficient  $R^2$  of RSB<sub>600</sub> and M-RSB<sub>600</sub> were 0.984 and 0.992, respectively, which were higher than other models. In addition, the theoretical  $q_e$  of RSB<sub>600</sub> and M-RSB<sub>600</sub> for MB was close to the measured  $q_e$  (152.32 mg/g and 255.77 mg/g), and the relative errors were only 6.42% and 4.96%, respectively, which indicated that the two RSBs' adsorption behavior for MB was more consistent with the quasi-second-order kinetic model, and chemical reaction primarily governed the adsorption process. The M-theoretical RSB<sub>600</sub>'s equilibrium adsorption capacity for MB was 65.6% more than RSB<sub>600</sub>'s. According to the research of Zhang et al. [45], the adsorption behavior of Cu(II) on cow manure biochar can be described by a quasi-second-order kinetic model, and the adsorption process was governed by surface complexation and coprecipitation. It was also discovered that the adsorption process followed the quasi-second-order kinetic model in a study by Hoslett et al. [46] on the removal of MB from water by biochar prepared by pyrolysis of mixed municipal solid waste. Its determination coefficient  $R^2$  was higher than the quasi-first-order and intraparticle diffusion model. According to the quasi-second-order kinetic model, chemical adsorption was the key rate-limiting step, but liquid film diffusion, surface adsorption and particle diffusion might also have an impact on the adsorption process.

**Table 3.** Adsorption kinetics fitting parameters of RSB<sub>600</sub> and M-RSB<sub>600</sub> for MB.

Analysis Item	Index	RSB <sub>600</sub>	M-RSB <sub>600</sub>
Quasi-first-order	$q_e$ (mg/g)	147.88	247.04
	$k_1$ (min <sup>-1</sup> )	0.10	0.11
	$R^2$	0.9698	0.9449
Quasi-second-order	$q_e$ (mg/g)	162.11	268.46
	$k_2$ [g/(mg·min)]	8.51	6.21
	$R^2$	0.984	0.992

Intraparticle diffusion	A	82.47	149.57
	$k_3$ [mg/(g·min <sup>0.5</sup> )]	6.51	9.88
	$R^2$	0.622	0.642
Elovich	B	39.98	85.87
	$k_4$ [mg/(g·min)]	24.22	36.55
	$R^2$	0.855	0.869

The MB adsorption quantity data was fitted in stages using the intraparticle diffusion model to further explore the rate-limiting step of clearance for MB in aqueous environment by RSB<sub>600</sub> and M-RSB<sub>600</sub>. Figure 10 displays the results of the more precise fitting.

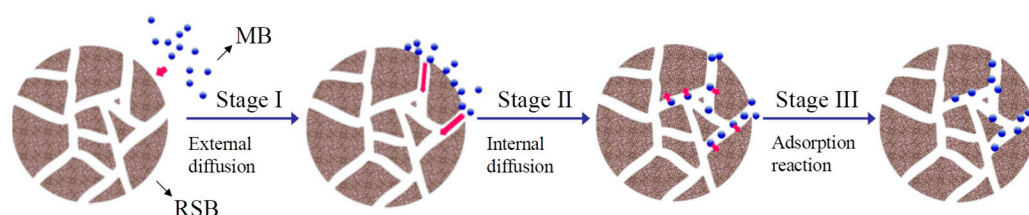


**Figure 10.** Staged fitting of intraparticle diffusion.

Table 4 displays the fitting parameters for each stage. As can be seen, there are three primary steps to the adsorption process of RSB for MB: exterior diffusion (stage I, lasting 0–30 min), internal diffusion (stage II, lasting 30–60 min) and adsorption reaction (stage III, lasting 60–180 min) [47]. In stage I, the MB content in the reaction system was high, the adsorption spots on the RSB were abundant and the MB diffused rapidly to the RSB surface through the liquid phase boundary membrane, which was a short and fast adsorption stage. This stage took a short time, and the adsorption was fast. In stage II, MB diffused to the internal pores of RSB under the external mass transfer driving force. Compared with the first stage, the adsorption rate constant  $k_3$  decreased significantly, and the adsorption rate started to slow down. Stage III saw a further prolongation of the reaction time that resulted in a low concentration of leftover MB in the solution and a progressive decrease in the number of remaining adsorption sites on the RSB. MB started to become attached to the inner part of RSB, and the attachment gradually became saturated. The adsorption process can be described in Figure 11. The  $k_3$  value of M-RSB<sub>600</sub> in stage I and II was 1.47 times and 1.54 times of RSB<sub>600</sub>, respectively, which again confirmed the advantage of higher adsorption efficiency of RSB after NaOH modification. It was precisely because it had completed the removal of MB more quickly and efficiently in the first 60 min that the  $k_3$  value of stage III decreased. Additionally, the fitting line in phases I–III had an A value greater than 0 and did not cross the coordinate axis origin, which indicated that the diffusion within the particles was not the only velocity-limiting cause for RSB adsorption to remove MB in water. The adsorption of MB by RSB<sub>600</sub> and M-RSB<sub>600</sub> was also affected by other processes such as liquid membrane diffusion and adsorption reaction [48].

**Table 4.** Staged fitting parameters of the intraparticle diffusion model.

Stage	Parameter	RSB <sub>600</sub>	M-RSB <sub>600</sub>
I	$A_1$	17.30	55.12
	$k_{31}$ [mg/(g·min <sup>0.5</sup> )]	22.18	32.54
	$R^2$	0.902	0.909
II	$A_2$	86.92	154.02
	$k_{32}$ [mg/(g·min <sup>0.5</sup> )]	8.01	12.33
	$R^2$	0.999	0.959
III	$A_3$	144.12	248.52
	$k_{33}$ [mg/(g·min <sup>0.5</sup> )]	0.62	0.53
	$R^2$	0.976	0.984

**Figure 11.** Adsorption process of MB onto RSB.

### 3.4. Adsorption Isotherm

The Langmuir, Freundlich and Temkin models [49], as illustrated in formulas (7)–(9), were used to fit the adsorption experimental data under various initial MB concentrations and reaction temperatures in order to examine the adsorption equilibrium connection between RSB and MB. Figure 12 displays the results of the fitting.

$$q_e = \frac{q_m K_L C_e}{1 + K_L C_e} \quad (7)$$

$$q_e = K_F C_e^{\frac{1}{n}} \quad (8)$$

$$q_e = K_T \ln C_e + C \quad (9)$$

where  $q_e$  and  $q_m$ , respectively, represent the equilibrium adsorption capacity and theoretical maximum adsorption capacity of MB (mg/g),  $C_e$  is the mass concentration of MB at the adsorption equilibrium (mg/L),  $K_L$  represents the adsorption equilibrium constant of the Langmuir model (L/mg),  $K_F$  ((mg<sup>1-1/n</sup>·L<sup>1/n</sup>)/g) and  $n$  represent the correlation constants of the Freundlich model,  $K_T$  (L/g) represents the equilibrium binding constant of the Temkin model and  $C$  represents the coefficient related to the adsorption heat.

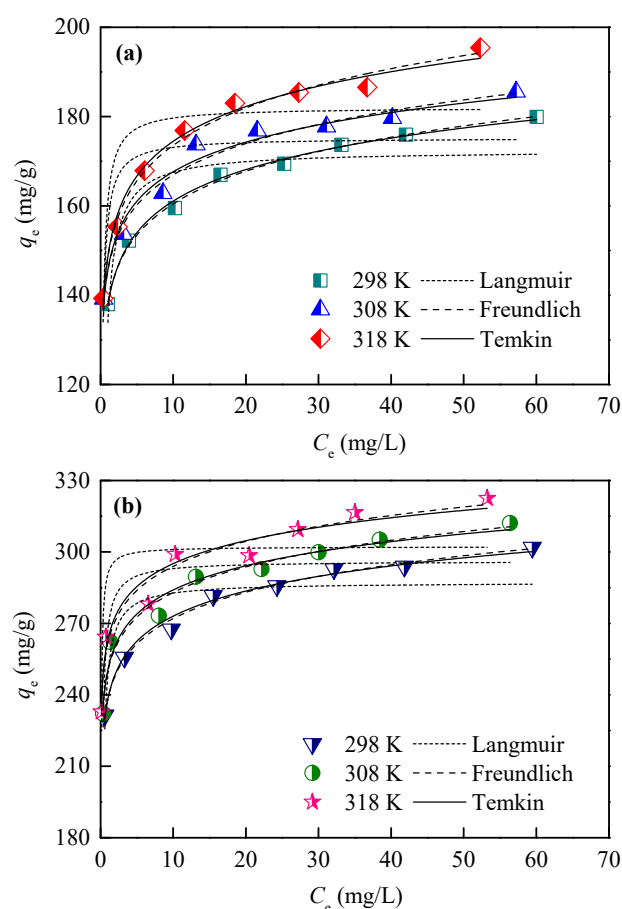


**Figure 12.** Isothermal adsorption fitting of RSB<sub>600</sub> (a) and M-RSB<sub>600</sub> (b) for MB.

Table 5 reflects the fitting parameters of the above three adsorption isotherm models. It is evident that, as the initial mass concentration of MB and reaction temperature increased, so did the amount of MB adsorb by RSB. The determination coefficients  $R^2$  obtained by fitting with Langmuir model were all lower than 0.8, indicating that this model was not appropriate for representing the MB's non-monolayer adsorption behavior on RSB [50]. The determination coefficients  $R^2$  fitted by the Freundlich and Temkin models were more than 0.95, indicating that the adsorption behavior was more suitable to be described by these two models. The Freundlich model reflected that the adsorption process of MB by RSB<sub>600</sub> and M-RSB<sub>600</sub> belonged to multilayer adsorption on a nonuniform surface [51]. According to the Temkin model, the reaction between MB and RSB brought about a linear decline in the adsorption heat of molecules under the same layer [52]. In the study of adsorption of microcystin-LR by iron-activated biochar, Zeng et al. found that not only the Freundlich model but also the Temkin model can better fit the experimental data, indicating that temperature had a significant role in heat exchange on adsorption process's [53]. This result was consistent with the conclusion of this study.

In addition, when the Freundlich model constant  $1/n$  value was less than 1, the adsorption process was prone to occur [54]. Meanwhile, the higher the  $K_F$  value, the better the adsorption performance of biochar [55]. In this study, the  $1/n$  value was less than 0.1, indicating that the adsorption of RSB<sub>600</sub> and M-RSB<sub>600</sub> for MB was successful, and even at low MB concentrations, a substantial adsorption efficiency could be achieved. The  $K_F$  value increased as the reaction temperature rose, indicating that higher temperatures were favorable for better RSB adsorption efficacy. This is due to the following reasons: (1) with the boost of temperature, the Brownian motion of MB rose significantly, which meant that MB was easier to enter the inner pores of RSB; (2) high temperatures accelerated the pace at which MB exchanged with other cations and (3) oxygen-containing functional

groups were activated by high temperature, which encouraged the creation of diverse chemical bonds. When utilizing NaOH-modified cactus biochar to adsorb contaminants from water, Choudhary et al. [56] discovered comparable outcomes. Again, demonstrating that NaOH modification can successfully improve RSB adsorption performance, the  $K_F$  value of M-RSB<sub>600</sub> ranged from 238.26 to 261.66, which was 1.72 to 1.76 times that of RSB<sub>600</sub>. This was closely related to the increased specific surface area and richer pore structure of RSB after alkali modification, which were both increased.

**Table 5.** Isothermal adsorption fitting parameters of RSB<sub>600</sub> and M-RSB<sub>600</sub> for MB.

Model	Parameter	RSB <sub>600</sub>			M-RSB <sub>600</sub>		
		298K	308K	318K	298K	308K	318K
Langmuir	$q_m$ (mg/g)	172.36	175.22	182.06	287.20	296.15	302.21
	$K_L$ (L/mg)	3.45	8.17	7.54	6.33	9.29	24.94
	$R^2$	0.779	0.664	0.676	0.714	0.774	0.684
Freundlich	$1/n$	0.064	0.060	0.068	0.058	0.054	0.051
	$K_F [(mg^{1-1/n} \cdot L^{1/n})/g]$	138.40	145.53	148.40	238.26	250.01	261.66
	$R^2$	0.995	0.975	0.990	0.991	0.965	0.958
Temkin	$C$	137.63	145.63	148.57	238.03	250.37	263.09
	$K_T$ (L/g)	10.18	9.56	11.24	15.21	14.63	13.90
	$R^2$	0.995	0.971	0.987	0.987	0.964	0.954

### 3.5. Adsorption Thermodynamics

For a better understanding of the thermodynamic properties of MB adsorption on two types of biochar, we fitted the experimental data of MB adsorption reactions obtained for RSB<sub>600</sub> and M-RSB<sub>600</sub> at reaction temperatures of 298, 308 and 318 K with the following equations [57]. Figure 13 and Table 6 display the findings.

$$\Delta G = -RT \ln K_e \quad (10)$$

$$\Delta G = \Delta H - T\Delta S \quad (11)$$

where  $\Delta G$  and  $\Delta H$ , respectively, represent the Gibbs free energy change and enthalpy change (kJ/mol),  $\Delta S$  represents entropy change (kJ/(mol·K)),  $R$  represents the gas constant (8.314 J/(mol·K)),  $T$  represents Kelvin temperature (K) and  $K_e$  represents the thermodynamic equilibrium constant. The value of  $K_e$  is calculated by  $q_e/C_e$ .

Table 6 shows that the  $\Delta G$  value was negative, demonstrating the spontaneous nature of the RSB's adsorption behavior for MB. The modified RSB had a stronger adsorption spontaneity and higher adsorption efficiency for MB, as evidenced by the fact that the  $\Delta G$  value of M-RSB<sub>600</sub> was higher than that of RSB<sub>600</sub> at the same reaction temperature [58]. The  $\Delta H$  readings were all positive, indicating an endothermic process for the adsorption of MB onto RSB. Increasing the reaction temperature can facilitate the adsorption. It is commonly accepted that the adsorption process is primarily physical adsorption when  $\Delta H$  is less than 20 kJ/mol, and the adsorption process is primarily chemical adsorption when  $\Delta H$  is larger than 20 kJ/mol, based on the kind of dominant reaction [59]. In this study, the  $\Delta H$  values of RSB<sub>600</sub> and M-RSB<sub>600</sub> were higher than 20 kJ/mol, so their adsorption processes for MB were both dominated by chemical adsorption. Moreover, the  $\Delta H$  value of M-RSB<sub>600</sub> was much higher than that of RSB<sub>600</sub>, which indicated that, in the process of eliminating MB by M-RSB<sub>600</sub>, the chemical adsorption predominated over RSB<sub>600</sub>, which also became an important reason for the improvement of the adsorption performance of NaOH modified RSB. Additionally, the  $\Delta S$  values were all positive, indicating that the process of MB adsorption by RSB<sub>600</sub> and M-RSB<sub>600</sub> was primarily driven by entropy and that the degree of chaos at the interface between the solid phase and the liquid phase increased throughout the adsorption process [60].

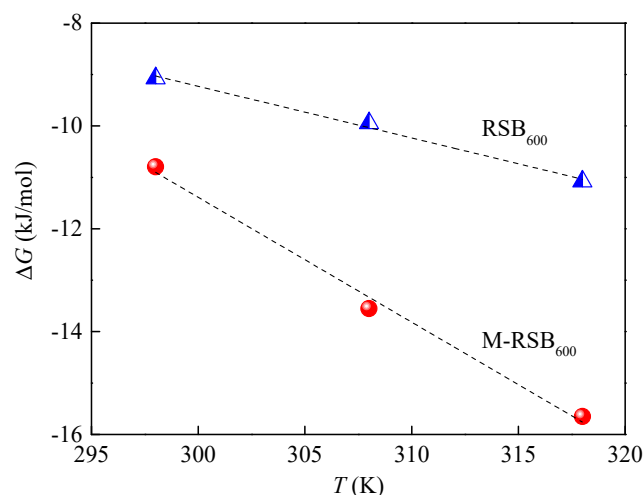


**Figure 13.** Adsorption thermodynamic fitting of RSB<sub>600</sub> and M-RSB<sub>600</sub> for MB.

**Table 6.** Adsorption thermodynamic parameters of RSB<sub>600</sub> and M-RSB<sub>600</sub> for MB.

Adsorbent	$\Delta G$ (kJ/mol)			$\Delta H$ (kJ/mol)	$\Delta S$ [kJ/(mol·K)]	$R^2$
	298K	308K	318K			
RSB <sub>600</sub>	-9.072	-9.947	-11.080	20.890	0.100	0.989
M-RSB <sub>600</sub>	-10.793	-13.551	-15.651	61.466	0.243	0.988

### 3.6. FTIR Comparison before and after Adsorption

The functional group structures on the surfaces of RSB<sub>600</sub> and M-RSB<sub>600</sub> before and after adsorption were examined in order to learn more about the adsorption mechanism of RSB<sub>600</sub> and M-RSB<sub>600</sub> for MB. The results are shown in Figure 14.

From Figure 14, it is evident that before MB adsorption, both RSB<sub>600</sub> and M-RSB<sub>600</sub>, contained rich functional groups, including –OH, C–H, C=C, C=O, C–C, Si–O–Si, etc., which created a good foundation for their adsorption of MB [61,62]. After MB adsorption, the –OH stretching vibration peak of RSB<sub>600</sub> moved from 3435 cm<sup>-1</sup> to 3439 cm<sup>-1</sup>, while the –OH stretching vibration peak of M-RSB<sub>600</sub> moved from 3440 cm<sup>-1</sup> to 3435 cm<sup>-1</sup>. This indicated that –OH on RSB may form a hydrogen bond with the aromatic ring on MB, thus changing the position of its stretching vibration peak [63]. The position of the C–H stretching vibration peak of RSB<sub>600</sub> did not change, while the C–H stretching vibration peak of M-RSB<sub>600</sub> moved from 2856 and 2924 cm<sup>-1</sup> to 2858 and 2926 cm<sup>-1</sup>, respectively, indicating that the adsorption process of M-RSB<sub>600</sub> was involved by these functional groups and played a crucial role in the process. The positions of C=C and C=O stretching vibration peaks of RSB<sub>600</sub> did not change, while the C=C and C=O stretching vibration peaks of M-RSB<sub>600</sub> moved from 1633 cm<sup>-1</sup> to 1632 cm<sup>-1</sup>, which indicated that there may be a  $\pi$ – $\pi$  bond between the aromatic ring structure of M-RSB<sub>600</sub> and MB [64,65]. The C–C stretching vibration peak of RSB<sub>600</sub> moved from 1398 cm<sup>-1</sup> to 1396 cm<sup>-1</sup>, while the C–C stretching vibration peak of M-RSB<sub>600</sub> moved from 1400 cm<sup>-1</sup> to 1396 cm<sup>-1</sup>. The Si–O–Si-bending vibration peak of RSB<sub>600</sub> moved from 1111 cm<sup>-1</sup> to 1117 cm<sup>-1</sup>, while the Si–O–Si-bending vibration peak of M-RSB<sub>600</sub> moved from 1095 cm<sup>-1</sup> to 1097 cm<sup>-1</sup>. The C–H-bending vibration peak position of RSB<sub>600</sub> did not change, while the C–H-bending vibration peak of M-RSB<sub>600</sub> moved from 725 cm<sup>-1</sup> to 721 cm<sup>-1</sup>. It can be seen that C–C, Si–O–Si and C–H all participated in the adsorption process of MB onto M-RSB<sub>600</sub> and played important roles in the adsorption process. In addition, MB existing in the form of a cation in water may also have an ion exchange interaction with trace exchangeable cations (such as Ca<sup>2+</sup>, Mg<sup>2+</sup>, K<sup>+</sup>, Na<sup>+</sup>, etc.) on RSB, which would also contribute to the improvement of the adsorption capacity [66]. However, the functional group distribution of RSB<sub>600</sub> was not as rich as that of M-RSB<sub>600</sub>,

and some functional groups did not participate in the reaction during the adsorption process, so its adsorption performance was poor compared with that of M-RSB<sub>600</sub>, which also confirmed the previous inference.

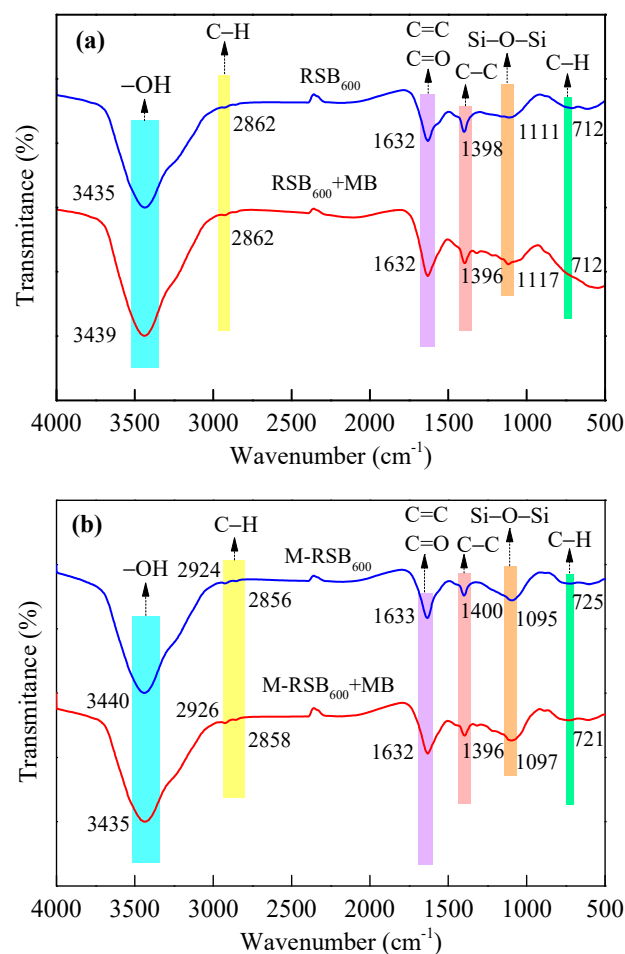


**Figure 14.** FTIR spectra of RSB<sub>600</sub> (a) and M-RSB<sub>600</sub> (b) before and after MB adsorption.

As shown in Figure 15, the adsorption mechanism of RSB for MB in aqueous solution mainly involved electrostatic attraction, a hydrogen bond, a  $\pi$ - $\pi$  bond and ion exchange. Multiple research projects have indicated that the removal of pollutants from water by biochar was a complex process. Gao et al. [67] prepared cotton straw biochar at the temperature of 250–650 °C to adsorb lead ions in water. It was found that the adsorption process involved six mechanisms, of which the most important adsorption mechanisms were precipitation, ion exchange,  $\text{Pb}^{2+}$ - $\pi$  interaction and complexation. Sahu et al. [68] used KOH modified litchi seed biochar to remove MB from water and confirmed that the primary adsorption processes were electrostatic interaction,  $\pi$ - $\pi$  interaction and hydrogen bond interactions. The intricate and distinct structural qualities of biochar provided favorable circumstances for the substance's adsorption of contaminants in water, and at the same time, a complex adsorption mechanism was formed, and the adsorption mechanism was different due to the different raw materials, preparation and modification conditions, adsorption conditions and types of target pollutants of biochar. The preparation and modification of RSB not only provided an alternative way for the reuse of waste rape straw but also opened up a new method for the removal of MB in water.

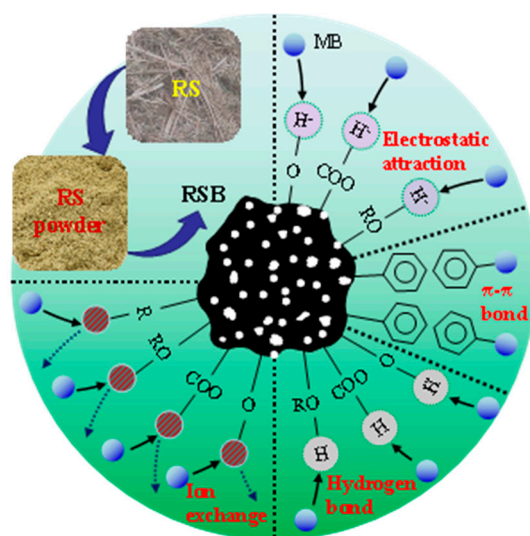


**Figure 15.** Adsorption mechanism of RSB for MB.

### 3.7. Analysis of Regeneration Effect

Figure 16 shows the change of MB removal rate by RSB<sub>600</sub> and M-RSB<sub>600</sub> under different recycling times. With the increase of recycling times, the MB removal rate showed a downward trend. After six cycles, the removal rate of MB by M-RSB<sub>600</sub> decreased to 81.45%. Although the removal rate of MB decreased, it still remained above 80%, indicating that the reusability of M-RSB<sub>600</sub> was good. The removal rate of MB by RSB<sub>600</sub> decreased to 70.58%, indicating that the reusability of unmodified RSB was relatively poor. In practical application, M-RSB<sub>600</sub> could effectively remove MB and could be reused for many times after regeneration, which was of better environmental and economic benefits.

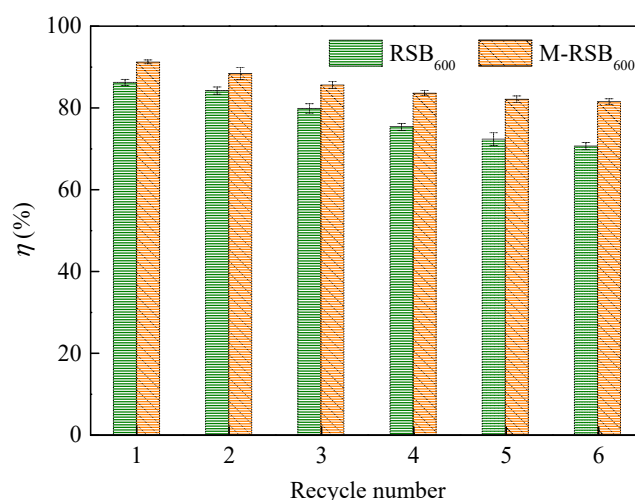


**Figure 16.** Desorption and regeneration effects of RSB<sub>600</sub> and M-RSB<sub>600</sub>.

Table 7 lists the adsorption capacity of several different types of biochar to MB. It can be seen that the adsorption capacity of the biochar prepared under the conditions of different biomass raw materials, pyrolysis temperatures and modifiers was different. RSB<sub>600</sub> in this study showed good MB adsorption performance without modification. The M-RSB<sub>600</sub> obtained after NaOH modification had a better MB adsorption performance than RSB<sub>600</sub>, showing greater application potential. The preparation and modification of RSB not only provided an alternative way for the reuse of waste rape straw but also opened up a new method for the removal of MB in water.

**Table 7.** Comparison of MB adsorption capacity by different types of biochar.

Type of Biochar	Pyrolysis Temperature (°C)	Modifying Agent	Adsorption Capacity (mg/g)	References
Rice husk	—	Zn/Al LDH	15.585	[18]
Sawdust	800	None	123.3	[20]
Cassava peel	300	SDBS	4.6916	[21]
Cotton residue	550	NaOH	23.82	[22]
Lychee seed	700	KOH	124.53	[68]
Tea residue	700	KOH + FeCl <sub>3</sub>	394.3	[69]
Tea residue	700	NaOH	105.44	[70]
Sewage sludge	600	None	51.1	[71]
RSB <sub>600</sub>	600	None	148.94	Present study
M-RSB <sub>600</sub>	600	NaOH	250.30	Present study

#### 4. Conclusions

This study explored the adsorption properties of rape straw biochar (RSB<sub>600</sub>) and NaOH modified rape straw biochar (M-RSB<sub>600</sub>) for MB in water. The characterization results of physical and chemical properties revealed that M-RSB<sub>600</sub> had greater aromaticity, higher hydrophilicity and polarity, as well as a larger specific surface area and total pore volume. The pores were also more numerous and tightly organized. The surface structure of RSB was obviously improved by alkali modification. The analysis results of adsorption influencing factors showed that the optimal initial pH of solution for the adsorption of MB by RSB<sub>600</sub> and M-RSB<sub>600</sub> was 10, and the alkaline environment was more favorable for the improvement of the adsorption effect. Under the same operating conditions, the dosage of M-RSB<sub>600</sub> required to achieve a similar MB effect was significantly lower than that of RSB<sub>600</sub>. The adsorption equilibrium time was about 60 min. The initial MB concentration can be appropriately increased to boost the absorptivity of RSB<sub>600</sub> and M-RSB<sub>600</sub> for MB.

The adsorption kinetics of MB on RSB<sub>600</sub> and M-RSB<sub>600</sub> were better explained by the quasi-second-order kinetic model, according to the finds of the kinetic study. External diffusion, internal diffusion and adsorption reaction made up the three steps of the adsorption process. These three phases had an impact on the adsorption rate. The isothermal adsorption investigation showed that the Temkin and Freundlich models can accurately reproduce the experimental results. The adsorption was mainly multilayer adsorption, and the temperature had an important effect on the adsorption heat. The findings of the thermodynamic study demonstrated that the adsorption of MB by RSB<sub>600</sub> and M-RSB<sub>600</sub> was an entropy-driven, spontaneous process and that the temperature rise was advantageous for enhancing the adsorption effect. M-RSB<sub>600</sub> had more surface functional groups than RSB<sub>600</sub>, according to the comparison results from FTIR, and more functional groups were involved in the adsorption reaction. Adsorption was a complicated process, and the ion exchange, hydrogen bond,  $\pi$ - $\pi$  bond and electrostatic attraction were all key components of the mechanism. Compared with RSB<sub>600</sub>, M-RSB<sub>600</sub> had a better regeneration performance. It can effectively solve the pollution problem of MB and waste rape straw and produce good environmental and economic benefits. The research on the removal of MB by making rape straw into biochar and alkali-modified biochar can effectively solve the pollution problem of MB and waste rape straw at the same time, resulting in good environmental and economic benefits.

**Author Contributions:** Conceptualization, Y.L. (Yixin Lu); Data curation, Y.L. (Yixin Lu) and J.C.; Formal analysis, J.C., C.T., Y.L. (Yujie Liu) and W.H.; Investigation, X.L. and J.S.; Methodology, Y.L. (Yixin Lu) and J.C.; Writing—original draft, J.C. and Writing—review and editing, C.T., Y.L. (Yujie Liu) and A.W. All authors have read and agreed to the published version of the manuscript.

**Funding:** This work was financially supported by the Sichuan Science and Technology Program (2022YFG0307), Natural Science Foundation of Sichuan Province (2022NSFSC0393), Open Fund of State Environmental Protection Key Laboratory of Synergetic Control and Joint Remediation for Soil

& Water Pollution (GHBK-2021-004), National College Students' Innovation Training Program (202211116025), University's Scientific Research Project of CDTU (2022ZR001), Young Seedling Program of CDTU (QM2021003) and Laboratory Open Fund Project of CDTU (2022CHZH04).

**Data Availability Statement:** Data are available on request from the authors.

**Conflicts of Interest:** The authors declare no conflict of interest.

## References

1. Bezzerrouk, M.A.; Bousmaha, M.; Hassan, M.; Akriche, A.; Guezzoul, M. Enhanced methylene blue removal efficiency of SnO<sub>2</sub> thin film using sono-photocatalytic processes. *Opt. Mater.* **2021**, *117*, 111116.
2. Zhang, Y.; Zheng, Y.; Yang, Y.; Huang, J.; Gao, B. Mechanisms and adsorption capacities of hydrogen peroxide modified ball milled biochar for the removal of methylene blue from aqueous solutions. *Bioresour. Technol.* **2021**, *337*, 125432.
3. Wang, F.; Yeap, S.P. Using magneto-adsorbent for methylene blue removal: A decision-making via analytical hierarchy process (AHP). *J. Water Process Eng.* **2021**, *40*, 101948.
4. Hu, Y.; Chen, D.; Wang, S.; Zhang, R.; Wang, Y.; Liu, M. Activation of peroxymonosulfate by nitrogen-doped porous carbon for efficient degradation of organic pollutants in water: Performance and mechanism. *Sep. Purif. Technol.* **2022**, *280*, 119791.
5. Lin, Q.; Zeng, G.; Pu, S.; Yan, G.; Luo, J.; Wan, Y.; Zhao, Z. A dual regulation strategy for MXene-based composite membrane to achieve photocatalytic self-cleaning properties and multi-functional applications. *Chem. Eng. J.* **2022**, *443*, 136335.
6. Lin, Q.; Zeng, G.; Yan, G.; Luo, J.; Cheng, X.; Zhao, Z.; Li, H. Self-cleaning photocatalytic MXene composite membrane for synergistically enhanced water treatment: Oil/water separation and dyes removal. *Chem. Eng. J.* **2022**, *427*, 131668.
7. Zeng, G.; Wei, K.; Zhang, H.; Zhang, J.; Lin, Q.; Cheng, X.; Sengupta, A.; Chiao, Y. Ultra-high oil-water separation membrane based on two-dimensional MXene (Ti<sub>3</sub>C<sub>2</sub>T<sub>x</sub>) by co-incorporation of halloysite nanotubes and polydopamine. *Appl. Clay Sci.* **2021**, *211*, 106177.
8. Choi, Y.K.; Srinivasan, R.; Kan, E. Facile and economical functionalized hay biochar with dairy effluent for adsorption of tetracycline. *Acs Omega* **2020**, *5*, 16521–16529.
9. Bekhoukh, A.; Moulefera, I.; Zeggai, F.Z.; Benyoucef, A.; Bachari, K. Anionic methyl orange removal from aqueous solutions by activated carbon reinforced conducting polyaniline as adsorbent: Synthesis, characterization, adsorption behavior, regeneration and kinetics study. *J. Polym. Environ.* **2022**, *30*, 886–895.
10. Thang, N.H.; Khang, D.S.; Hai, T.D.; Nga, D.T.; Tuan, P.D. Methylene blue adsorption mechanism of activated carbon synthesised from cashew nut shells. *RSC Adv.* **2021**, *11*, 26563–26570.
11. Liu, X.J.; Li, M.F.; Singh, S.K. Manganese-modified lignin biochar as adsorbent for removal of methylene blue. *J. Mater. Res. Technol.* **2021**, *12*, 1434–1445.
12. Li, F.; Liu, J.; Liu, W.; Xu, Y.; Xu, M. Preparation of hyper-cross-linked hydroxylated polystyrene for adsorptive removal of methylene blue. *RSC Adv.* **2021**, *11*, 25551–25560.
13. Al-Aoh, H.A.; Aljohani, M.; Darwish, A.; Ahmad, M.A.; Bani-Atta, S.A.; Al-sharif, M.A.; Alrawashdeh, L.R.; Al-Tweher, J.N. A potentially low-cost adsorbent for methylene blue removal from synthetic wastewater. *Desalin. Water Treat.* **2021**, *213*, 431–440.
14. Toumi, I.; Djelad, H.; Chouli, F.; Benyoucef, A. Synthesis of PANI@ZnO hybrid material and evaluations in adsorption of congo red and methylene blue dyes: Structural characterization and adsorption performance. *J. Inorg. Organomet. P.* **2022**, *32*, 112–121.
15. Wei, S.; Wu, J.; Chen, P.; Fu, B.; Zhu, X.; Chen, M. Integration of phosphotungstic acid into zeolitic imidazole framework-67 for efficient methylene blue adsorption. *ACS Omega* **2022**, *7*, 9900–9908.
16. Gao, Y.A.; Sun, D.I.; Han, C.; Huang, J. Comprehensive utilization of phosphogypsum: Adsorption of methylene blue and its application in bricks. *Surf. Rev. Lett.* **2021**, *28*, 2150075.
17. Li, N.; He, M.; Lu, X.; Yan, B.; Duan, X.; Chen, G.; Wang, S.; Hou, L. Municipal solid waste derived biochars for wastewater treatment: Production, properties and applications. *Resour. Conserv. Recy.* **2022**, *177*, 106003.
18. Lesbani, A.; Siregar, P.; Palapa, N.R.; Taher, T.; Riyanti, F. Adsorptive removal methylene-blue using Zn/Al LDH modified rice husk biochar. *Pol. J. Environ. Stud.* **2021**, *30*, 3117–3124.
19. Wang, Y.; Srinivasakannan, C.; Wang, H.; Xue, G.; Wang, L.; Wang, X.; Duan, X. Preparation of novel biochar containing graphene from waste bamboo with high methylene blue adsorption capacity. *Diam. Relat. Mater.* **2022**, *125*, 109034.
20. Amin, M.T.; Alazba, A.A.; Shafiq, M. Successful application of eucalyptus camdulensis biochar in the batch adsorption of crystal violet and methylene blue dyes from aqueous solution. *Sustainability* **2021**, *13*, 3600.
21. Anas, A.K.; Pratama, S.Y.; Izzah, A.; Kurniawan, M.A. Sodium dodecylbenzene sulfonate-modified biochar as an adsorbent for the removal of methylene blue. *Bull. Chem. React. Eng.* **2021**, *16*, 188–195.
22. Primaz, C.T.; Ribes-Greus, A.; Jacques, R.A. Valorization of cotton residues for production of bio-oil and engineered biochar. *Energy* **2021**, *235*, 121363.
23. Yang, Z.; Hou, J.; Miao, L.; Wu, J. Comparison of adsorption behavior studies of methylene blue by microalga residue and its biochars produced at different pyrolytic temperatures. *Environ. Sci. Pollut. Res.* **2021**, *28*, 14028–14040.
24. Suma, Y.; Pasukphun, N.; Eaktasang, N. Adsorption of methylene blue by low-cost biochar derived from elephant dung. *Appl. Environ. Res.* **2021**, *43*, 34–44.

25. Yin, Q.; Nie, Y.; Han, Y.; Wang, R.; Zhao, Z. Properties and the application of sludge-based biochar in the removal of phosphate and methylene blue from water: Effects of acid treating. *Langmuir* **2022**, *38*, 1833–1844.
26. Zhang, X.; Zheng, H.; Wu, J.; Chen, W.; Chen, Y.; Gao, X.; Yang, H.; Chen, H. Physicochemical and adsorption properties of biochar from biomass-based pyrolytic polygeneration: Effects of biomass species and temperature. *Biochar* **2021**, *4*, 657–670.
27. Huang, L.; Zhu, Y.; Wang, Q.; Zhu, A.; Li, L. Assessment of the effects of straw burning bans in China: Emissions, air quality, and health impacts. *Sci. Total Environ.* **2021**, *789*, 147935.
28. Cui, S.B.; Zhao, Y.; Liu, Y.; Huang, R.; Pan, J. Preparation of straw porous biochars by microwave-assisted KOH activation for removal of gaseous H<sub>2</sub>S. *Energy Fuels* **2021**, *35*, 18592–18603.
29. Magid, A.; Islam, M.S.; Chen, Y.; Weng, L.; Li, Y. Enhanced adsorption of polystyrene nanoplastics (PSNPs) onto oxidized corn cob biochar with high pyrolysis temperature. *Sci. Total Environ.* **2021**, *784*, 147115.
30. Pandey, D.; Daverey, A.; Dutta, K.; Yata, V.K.; Arunachalam, K. Valorization of waste pine needle biomass into biosorbents for the removal of methylene blue dye from water: Kinetics, equilibrium and thermodynamics study. *Environ. Technol. Innov.* **2022**, *25*, 102200.
31. Wang, Z.; Jang, H.M. Comparative study on characteristics and mechanism of levofloxacin adsorption on swine manure biochar. *Bioresour. Technol.* **2022**, *351*, 127025.
32. Shin, J.; Lee, Y.G.; Lee, S.H.; Kim, S.; Chon, K. Single and competitive adsorptions of micropollutants using pristine and alkali-modified biochars from spent coffee grounds. *J. Hazard. Mater.* **2020**, *400*, 123102.
33. Novera, T.M.; Tabassum, M.; Bardhan, M.; Islam, M.A.; Islam, M.A. Chemical modification of betel nut husk prepared by sodium hydroxide for methylene blue adsorption. *Appl. Water Sci.* **2021**, *11*, 66.
34. Huang, W.; Zhang, M.; Wang, Y.; Chen, J.; Zhang, J. Biochars prepared from rabbit manure for the adsorption of Rhodamine B and Congo red: Characterization, kinetics, isotherms, and thermodynamic studies. *Water Sci. Technol.* **2020**, *81*, 436–444.
35. Lu, Y.; Chen, J.; Zhao, L.; Zhou, Z.; Qiu, C.; Li, Q. Adsorption of Rhodamine B from aqueous solution by goat manure biochar: Kinetics, isotherms, and thermodynamic studies. *Pol. J. Environ. Stud.* **2020**, *29*, 2721–2730.
36. Konicki, W.; Aleksandrak, M.; Mijowska, E. Equilibrium, kinetic and thermodynamic studies on adsorption of cationic dyes from aqueous solutions using graphene oxide. *Chem. Eng. Res. Des.* **2017**, *123*, 35–49.
37. Huang, W.; Chen, J.; Zhang, J. Adsorption characteristics of methylene blue by biochar prepared using sheep, rabbit and pig manure. *Environ. Sci. Pollut. Res.* **2018**, *25*, 29256–29266.
38. Salah, J.; Amine, A.A.; Majida, A.; Yassine, C.; Nasser, A.J.; Ahmed, A.; Muhammad, U.; Noura, A.N.; Mohammed, A.A.; Mejd, J. Conversion of industrial sludge into activated biochar for effective cationic dye removal: Characterization and adsorption properties assessment. *Water* **2022**, *14*, 2206.
39. Taheri, E.; Fatehizadeh, A.; Lima, E.C.; Rezakazemi, M. High surface area acid-treated biochar from pomegranate husk for 2,4-dichlorophenol adsorption from aqueous solution. *Chemosphere* **2022**, *295*, 133850.
40. Huang, W.; Chen, J.; Zhang, J. Removal of ciprofloxacin from aqueous solution by rabbit manure biochar. *Environ. Technol.* **2020**, *41*, 1380–1390.
41. Wang, F.; Li, L.; Iqbal, J.; Yang, Z.; Du, Y. Preparation of magnetic chitosan corn straw biochar and its application in adsorption of amaranth dye in aqueous solution. *Int. J. Biol. Macromol.* **2022**, *199*, 234–242.
42. Lu, Y.; Chen, J.; Zhang, J.; Fu, C. Kinetic, isotherm and thermodynamic studies on the adsorption behavior of atrazine onto sheep manure-derived biochar. *Pol. J. Environ. Stud.* **2019**, *28*, 2725–2733.
43. Cai, G.; Ye, Z. Concentration-dependent adsorption behaviors and mechanisms for ammonium and phosphate removal by optimized Mg-impregnated biochar. *J. Clean. Prod.* **2022**, *349*, 131453.
44. Palansooriya, K.N.; Kim, S.; Igalavithana, A.D.; Hashimoto, Y.; Choi, Y.; Mukhopadhyay, R.; Sarkar, B.; Ok, Y.S. Fe(III) loaded chitosan-biochar composite fibers for the removal of phosphate from water. *J. Hazard. Mater.* **2021**, *415*, 125464.
45. Zhang, P.; Zhang, X.; Yuan, X.; Xie, R.; Han, L. Characteristics, adsorption behaviors, Cu(II) adsorption mechanisms by cow manure biochar derived at various pyrolysis temperatures. *Bioresour. Technol.* **2021**, *331*, 125013.
46. Hoslett, J.; Ghazal, H.; Mohamad, N.; Jouhara, H. Removal of methylene blue from aqueous solutions by biochar prepared from the pyrolysis of mixed municipal discarded material. *Sci. Total Environ.* **2020**, *714*, 136832.
47. Li, H.; Xiong, J.; Zhang, G.; Liang, A.; Long, J.; Xiao, T.; Chen, Y.; Zhang, P.; Liao, D.; Lin, L.; et al. Enhanced thallium (I) removal from wastewater using hypochlorite oxidation coupled with magnetite-based biochar adsorption. *Sci. Total Environ.* **2020**, *698*, 134166.
48. Lu, Y.; Chen, J.; Bai, Y.; Gao, J.; Peng, M. Adsorption properties of methyl orange in water by sheep manure biochar. *Pol. J. Environ. Stud.* **2019**, *28*, 3791–3797.
49. Hu, Y.; Zhu, Y.; Zhang, Y.; Lin, T.; Long, H. An efficient adsorbent: Simultaneous activated and magnetic ZnO doped biochar derived from camphor leaves for ciprofloxacin adsorption. *Bioresour. Technol.* **2019**, *288*, 121511.
50. Mariia, G.; Alicja, B.; Dariusz, S.; Viktor, B.; Olena, O.; Gun'ko, V.; DeryłoMarczewska, A. Development, synthesis and characterization of tannin/bentonite-derived biochar for water and wastewater treatment from methylene blue. *Water* **2022**, *14*, 2407.
51. Bardhan, M.; Novera, T.M.; Tabassum, M.; Islam, M.A.; Jawad, A.H.; Islam, M.A. Adsorption of methylene blue onto betel nut husk-based activated carbon prepared by sodium hydroxide activation process. *Water Sci. Technol.* **2020**, *82*, 1932–1949.
52. Yan, L.; Liu, Y.; Zhang, Y.; Liu, S.; Wang, C.; Chen, W.; Liu, C.; Chen, Z.; Zhang, Y. ZnCl<sub>2</sub> modified biochar derived from aerobic granular sludge for developed microporosity and enhanced adsorption to tetracycline. *Bioresour. Technol.* **2020**, *297*, 122381.

53. Zeng, S.; Kan, E. Adsorption and regeneration on iron-activated biochar for removal of microcystin-LR. *Chemosphere* **2021**, *273*, 129649.
54. Zhang, Z.; Yan, L.; Yu, H.; Yan, T.; Li, X. Adsorption of phosphate from aqueous solution by vegetable biochar/layered double oxides: Fast removal and mechanistic studies. *Bioresour. Technol.* **2019**, *284*, 65–71.
55. Sun, D.; Li, F.; Jin, J.; Khan, S.; Eltohamy, K.M.; He, M.; Liang, X. Qualitative and quantitative investigation on adsorption mechanisms of Cd(II) on modified biochar derived from co-pyrolysis of straw and sodium phytate. *Sci. Total Environ.* **2022**, *829*, 154599.
56. Choudhary, M.; Kumar, R.; Neogi, S. Activated biochar derived from *Opuntia ficus-indica* for the efficient adsorption of malachite green dye, Cu<sup>2+</sup> and Ni<sup>2+</sup> from water. *J. Hazard. Mater.* **2020**, *392*, 122441.
57. Shi, W.; Wang, H.; Yan, J.; Shan, L.; Quan, G.; Pan, X.; Cui, L. Wheat straw derived biochar with hierarchically porous structure for bisphenol A removal: Preparation, characterization, and adsorption properties. *Sep. Purif. Technol.* **2022**, *289*, 120796.
58. Hu, H.; Zhang, J.; Wang, T.; Wang, P. Adsorption of toxic metal ion in agricultural wastewater by torrefaction biochar from bamboo shoot shell. *J. Clean. Prod.* **2022**, *338*, 130558.
59. Hernandez, P.T.; Franco, D.S.P.; Georjgin, J.; Salau, N.P.G.; Dotto, G.L. Investigation of biochar from *Cedrella fissilis* applied to the adsorption of atrazine herbicide from an aqueous medium. *J. Environ. Chem. Eng.* **2022**, *10*, 107408.
60. Wang, S.; Zhong, S.; Zheng, X.; Xiao, D.; Zhang, L.; Yang, Y.; Zhang, H.; Ai, B.; Sheng, Z. Calcite modification of agricultural waste biochar highly improves the adsorption of Cu(II) from aqueous solutions. *J. Environ. Chem. Eng.* **2021**, *9*, 106215.
61. Huang, H.; Zheng, Y.; Wei, D.; Yang, G.; Peng, X.; Fan, L.; Luo, L.; Zhou, Y. Efficient removal of pefloxacin from aqueous solution by acid–alkali modified sludge-based biochar: Adsorption kinetics, isotherm, thermodynamics, and mechanism. *Environ. Sci. Pollut. Res.* **2022**, *29*, 43201–43211.
62. Li, Y.; Chen, X.; Liu, L.; Liu, P.; Zhou, Z.; Huhetaoli; Wu, Y.; Lei, T. Characteristics and adsorption of Cr(VI) of biochar pyrolyzed from landfill leachate sludge. *J. Anal. Appl. Pyrol.* **2022**, *162*, 105449.
63. Liu, P.; Zhang, A.; Liu, Y.; Liu, Z.; Liu, X.; Yang, L.; Yang, Z. Adsorption mechanism of high-concentration ammonium by Chinese natural zeolite with experimental optimization and theoretical computation. *Water* **2022**, *14*, 2413.
64. Cheng, Y.; Wang, B.; Shen, J.; Yan, P.; Kang, J.; Wang, W.; Bi, L.; Zhu, X.; Wang, S.; Shen, L.; et al. Preparation of novel N-doped biochar and its high adsorption capacity for atrazine based on  $\pi$ – $\pi$  electron donor-acceptor interaction. *J. Hazard. Mater.* **2022**, *432*, 128757.
65. Xu, Z.; Xiang, Y.; Zhou, H.; Yang, J.; Zhou, Y. Manganese ferrite modified biochar from vinasse for enhanced adsorption of levofloxacin: Effects and mechanisms. *Environ. Pollut.* **2021**, *272*, 115968.
66. Zubair, M.; Mu'azu, N.D.; Jarrah, N.; Blaisi, N.I.; Aziz, H.A.; Al-Harhi, M.A. Adsorption behavior and mechanism of methylene blue, crystal violet, Eriochrome Black T, and methyl orange dyes onto biochar-derived. *Water Air Soil Poll.* **2020**, *231*, 240.
67. Gao, L.; Li, Z.; Yi, W.; Li, Y.; Wang, L. Impacts of pyrolysis temperature on lead adsorption by cotton stalk-derived biochar and related mechanisms. *J. Environ. Chem. Eng.* **2021**, *9*, 105602.
68. Sahu, S.; Pahi, S.; Tripathy, S.; Singh, S.K.; Patel, R.K. Adsorption of methylene blue on chemically modified lychee seed biochar: Dynamic, equilibrium, and thermodynamic study. *J. Mol. Liq.* **2020**, *315*, 113743.
69. Mu, Y.; Du, H.; He, W.; Ma, H. Functionalized mesoporous magnetic biochar for methylene blue removal: Performance assessment and mechanism exploration. *Diam. Relat. Mater.* **2022**, *121*, 108795.
70. Mu, Y.; Ma, H. NaOH-modified mesoporous biochar derived from tea residue for methylene blue and Orange II removal. *Chem. Eng. Res. Des.* **2021**, *167*, 129–140.
71. Ribeiro, M.R.; de Moraes Guimarães, Y.; Silva, I.F.; Almeida, C.A.; Silva, M.S.V.; Nascimento, M.A.; da Silva, U.P.; Varejão, E.V.; dos Santos Renato, N.; de Carvalho Teixeira, A.P.; et al. Synthesis of value-added materials from the sewage sludge of cosmetics industry effluent treatment plant. *J. Environ. Chem. Eng.* **2021**, *9*, 105367.